



Correlations between product distribution and feedstock composition in thermal cracking processes for mixed plastic waste

Downloaded from: <https://research.chalmers.se>, 2025-12-05 03:11 UTC

Citation for the original published paper (version of record):

Forero Franco, R., Cañete Vela, I., Berdugo Vilches, T. et al (2023). Correlations between product distribution and feedstock composition in thermal cracking processes for mixed plastic waste. Fuel, 341. <http://dx.doi.org/10.1016/j.fuel.2023.127660>

N.B. When citing this work, cite the original published paper.



Correlations between product distribution and feedstock composition in thermal cracking processes for mixed plastic waste

Renesteban Forero-Franco^{*}, Isabel Cañete-Vela, Teresa Berdugo-Vilches, Judith González-Arias, Jelena Maric, Henrik Thunman, Martin Seemann

Department of Space, Earth and Environment, Division of Energy Technology, Chalmers University of Technology, Gothenburg SE-41296, Sweden

ARTICLE INFO

Keywords:

Plastic waste recycling
Pyrolysis
Plastic waste composition
Convex optimization
Correlation analysis
Monomer Recovery

ABSTRACT

Thermal conversion can transform the carbon-based waste into valuable chemicals to be further used in the petrochemical industry for a polymeric carbon circular economy. This work's aim was to identify chemical correlations between the thermal-cracking products and the feedstock polymer composition when using highly blended waste streams. The challenges addressed were to: (i) access a pool of experimental data on the monomer recovery potential of real-life, highly blended waste streams; (ii) estimate the polymer constituents of the mixed waste streams; and (iii) formulate a generic and systematic method to identify correlations between feedstock constituents and cracking products. Different post-consumer waste streams were investigated, including cardboard, automotive shredder residues, cable stripping waste, and textile waste. The cracking experiments were performed in a 2–4MW_{th} industrial-scale Dual Fluidized Bed system at 800 °C using steam as fluidization agent. The polymeric constituents of the feedstocks were estimated using a numerical convex optimization method. To identify correlations between the feedstocks and products, a carbon bond-based classification was introduced. The experimental monomer yield ranged from 0.08 kg/kgf to 0.3 kg/kgf (f = feedstock) for the evaluated materials, corresponding to a carbon feedstock conversion rate between 14 % and 44 %. High yields of valuable monomers were obtained for the materials with the highest polyolefin content. The olefin monomer production correlated positively to the amount of aliphatic carbon in the original material and negatively to the carbon contents of the aromatic rings. From the trends observed, it was concluded that a framework based on carbon bond types is a promising approach to identify such correlations, which could serve as predictive tools for monomer recovery based on material's composition and overall process conditions.

1. Introduction

Polymer-rich waste fractions are of interest to the chemical industry as substitutes for virgin feedstocks [1–5]. Currently, several chemical recycling processes are being developed or under demonstration [2,6]. While the collection of polymer-based waste materials in Europe is extensive, current recycling systems are based on mechanical recycling (re-melting) and require homogeneous fractions in terms of the polymer type to present a clear value chain [7]. However, inherent to the products derived from mechanical recycling is the degradation of the properties of the material within the process. Chemical recycling, via either pyrolysis or solvolysis processes, can be considered as a complement to mechanical recycling. It is based on decomposition of the polymer into monomers or other smaller molecules, from which the polymer can be built anew at the highest quality levels. As the decomposition conditions

and products are polymer-dependent, most of the technologies are tailored to specific polymer types. As a consequence, the fractions of interest for both mechanical recycling technologies and chemical recycling technologies are predominantly polyolefins and polyethylene terephthalate (PET) by volume [7].

The restriction to relatively homogeneous feedstocks is, however, not consistent with the heterogeneity of real plastic waste streams. This mismatch between feedstock heterogeneity and applied technologies creates a high rate of rejection among of highly blended polymer mixtures. These rejects cannot be recycled with reasonable separation and sorting efforts and cannot be recycled into high-quality materials using current technologies [8]. Indeed, mixed polymeric waste may contain both synthetic polymers (plastics) and biopolymers (e.g., cellulose, natural rubber), either as composites or as a blend. Well-known examples are beverage cartons and textiles. In these examples, the

^{*} Corresponding author.

E-mail address: rforero@chalmers.se (R. Forero-Franco).

<https://doi.org/10.1016/j.fuel.2023.127660>

Received 1 November 2022; Received in revised form 29 December 2022; Accepted 30 January 2023

Available online 17 February 2023

0016-2361/© 2023 The Author(s). Published by Elsevier Ltd. This is an open access article under the CC BY license (<http://creativecommons.org/licenses/by/4.0/>).

functionality or the need for extended durability, rather than end-of-life considerations, dictates the choice of polymer material. Currently, these fractions are to a large extent energy-recovered through incineration. Thus, recycling back to materials might be possible via carbon capture and utilization (CCU), with the usage of hydrogen from electrolysis. Therefore, it can be regarded as a general recycling process, in contrast to the selective recycling methods discussed above.

To limit the thermodynamic penalty of the above-mentioned combustion route, thermal cracking and sorting of the final product distribution are proposed as an alternative. This method makes the entire carbon resource of a material blend available to the chemical industry and for new material production [9]. To allow separation of the final products from a heterogeneous feedstock into valuable fractions, the choice of operational conditions reflects a tradeoff between the decomposition of all troublesome or harmful components and the preservation of as much of the valuable hydrocarbons as possible. In thermal cracking, the aim is to decompose the macromolecules into smaller molecules while preserving parts of the structure. Ideally, high heating rates and high reaction temperatures promote cracking by triggering primary reactions that form products through decomposition of the polymer chains, which occurs through bond breakage and free radical mechanisms. Thereafter, secondary reactions with the products of the primary reactions take place in the gas phase. During this stage, volatiles can evolve to more-complex structures such as polyaromatics, and eventually soot. In addition, they can undergo further decomposition in reforming reactions towards syngas ($H_2 + CO$), in the presence of a poor oxidative medium, e.g., steam. Fig. 1 shows a schematic representation of this decomposition process. [10,11].

Although it is difficult to decouple the primary and secondary reactions, the process temperature and residence times are critical variables in modulating their chemistry and promoting a particular product distribution. In general, the temperature-induced breakages induced by free radicals during the primary reactions tend to break down the polymeric chain into the monomeric structures. In fact, the yields of monomers obtained from a cracking process rely heavily on driving the primary reactions and limiting the secondary reactions. Nonetheless, controlled secondary reactions are also important, as they can promote cyclization and generate valuable aromatic compounds additional to those present in the original chain. This is the case for aliphatic polymers such as PE, PP or PVC, which through cyclization reactions (e.g., Diels-

Alder cyclization) yield a product portfolio that includes economically valuable aromatics such as benzene, toluene, styrene and xylene [12–15]. Mixed wastes that contain these polymers can be expected to yield high concentrations of aromatics, despite the lack of aromatic structures in the feedstock polymer.

The cracking reactions are endothermic in nature, which means that energy must be added to the reactor in which the conversion is taking place. To drive the desired conversion reactions and to limit unwanted reactions, it is advantageous to have swift heating of the feedstock, a short residence time for the formed gases, and *in situ* dilution of the products. A reactor concept that captures these conditions is the allothermally heated stationary fluidized bed, fluidized with steam. Several options for allothermal heated fluidized beds have been developed [6,16–20]. Dual fluidized bed (DFB) systems consist of a combustor and a pyrolysis reactor, with the heated sand bed being used as a heat carrier between the reactors. Such twin-bed systems, apart from their intrinsic heating, offer the advantage of completing the conversion of char in the combustion section, together with continuous regeneration of the bed material. This allows for optimization of the reaction conditions for the preferred polymer conversion reactions to monomeric structures at temperatures that are too low for the conversion of char. Integration of such a system with a petrochemical site that replaces traditional steam crackers has been presented in a paper by Thunman et al. [9], which even discusses the possibility to employ biomass as an additional feedstock source for the process.

Despite the evident potential of chemical recycling to contribute to closed-loop resource use [21], its environmental benefits, in terms of global warming reduction potential and other impacts, are intensely debated and various authors have highlighted the need for real-process data to support decision-making processes. In this respect, information related to assessing chemical recycling via thermal cracking of polymer wastes with high olefinic contents into the building blocks of olefins is accumulating in the literature, and these processes are the subject of ongoing research projects [9,12,13,18,22,23]. In contrast, data relevant to the thermal cracking of mixed polymeric wastes with low contents of olefins or high contents of heteroatoms is scarce. Such wastes have not yet been addressed sufficiently due to their extreme diversity, such that their recycling potentials and possible value chains remain unclear.

The polymeric composition of a feedstock blend is an essential factor in determining the distribution of the products generated under specific

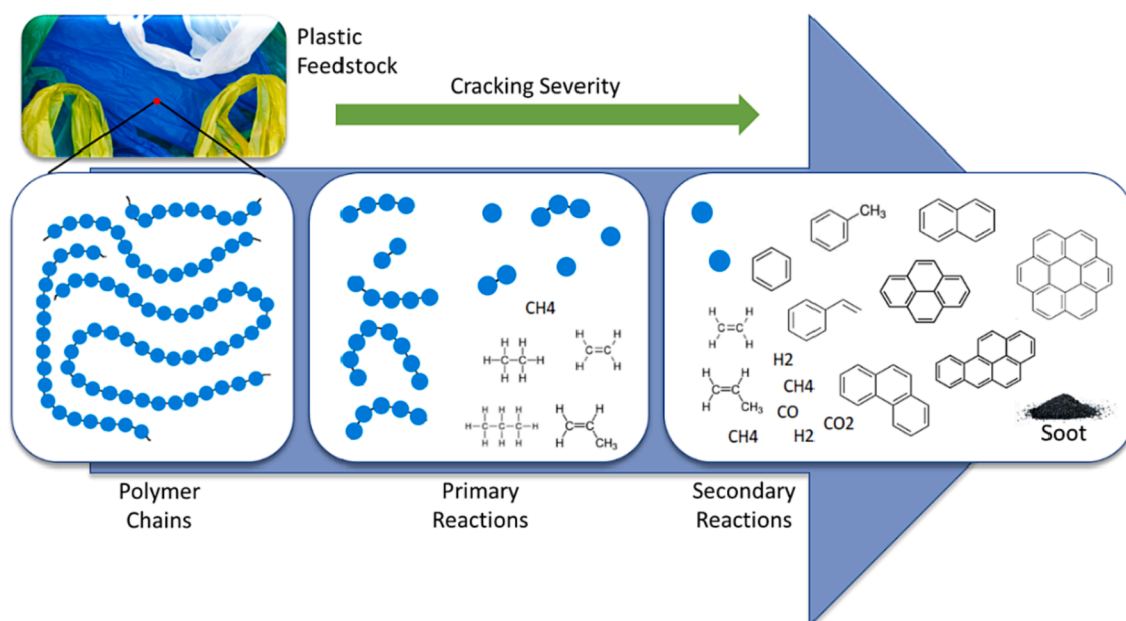


Fig. 1. Polymer chain decomposition through primary and secondary reactions in the cracking process.

operational conditions. However, in reality, the polymeric composition is usually not known, especially in the case of waste streams. Therefore, to estimate the original polymeric blend, direct characterization or numerical models based on easily available information are options that can be used. Direct characterization methods usually involve spectroscopic analyses, e.g., X-ray diffraction, Raman spectroscopy, and FT-IR or NIR spectrometry [24–26]. Yet, when dealing with particularly heterogeneous mixtures, these techniques give insufficient information regarding the bulk composition, due to the presence of composites, polymers with fillers, differently colored materials, and high ash contents. Thus, preprocessing of the feedstock is necessary to enable clean screening of the fractions, making the entire procedure time-consuming or effort-demanding, and requiring the use of expensive, multiple items of equipment for the characterization. In contrast, numerical models use formulations to derive a surrogate estimation of the plastic blend that is consistent with the mass and energy conservation laws [27]. Thus, such models provide a cheaper and faster way to arrive at physically congruent approximations of the polymer composition without the need for specialized and costly items of equipment.

The input blend and their main products when subjected to specific thermodynamic conditions can be useful for predictive purposes. Indeed, attempts to model the conversion behaviors of carbon-based materials have been proposed, together with the evaluation of surrogate polymeric formulations, which can follow the kinetic evolution pathways of certain key species and predict their final concentrations [27]. However, if information on the product distribution is also available, the preferred cleavage positions along the chain dictated by the incoming polymer's molecular structure gives valuable information that can be used to establish correlations that facilitate an understanding of how the different carbon bonds in the polymer blend can react and become transformed during the conversion process. This important knowledge about the monomer and chemical recovery potentials of the different plastics, as well as mixtures thereof, can be used to evaluate recycling routes and value chain possibilities.

Mixed waste materials have been studied by several research groups in pyrolysis and gasification processes at relatively small scales for fuels and energy recovery applications [6,14,23,28]. In the present work, experiments were conducted in an industrial-scale 2–4-MW cracker in a DFB plant to collect data on the thermo-cracking of a set of highly mixed polymer-rich wastes. The waste materials used were residual fractions of post-consumer products, which are difficult to recycle by mechanical means. The aim of this work was to identify qualitative correlations between the feedstock's polymeric composition and the distribution of products from the cracking. To this aim, a novel approach is introduced based on a carbon-based molecular classification of products and feedstock, so as to create a generalization framework within which the correlations could be studied. The cracking data were evaluated with respect to mass yields and carbon conversion ratios, to determine and compare each material's recycling potential with regard to their total monomeric yields. Additionally, since the polymeric compositions of the wastes were unknown, a statistical method based on convex optimization was applied to estimate numerically the compositions of the feedstock blends using information of the proximate and ultimate analyses.

The formulated generalization framework can be regarded as the initial step towards the development of predictive mathematical tools for thermal-cracking conversion, providing a map that links the chemical characteristics of the upstream and downstream species, and thereby providing an estimation of the potential monomer recovery yields of feedstock blends under specific process conditions.

2. Polymer types and cracking behaviors

2.1. Polymer types in waste streams

A polymeric waste stream is normally characterized by a heterogeneous blend of different plastic compounds, such as Polyethylene (PE),

Polypropylene (PP), Polyvinylchloride (PVC), and Polyethylene terephthalate (PET), among others. Even though a waste stream can be sorted to essentially a single polymer type, polymeric waste cannot be an entirely homogeneous material. Even if the basic monomer of two materials is the same, the polymers are functionalized, dyed, protected against ageing, and loaded with fillers so as to tailor the material properties to the function, which creates remnant heterogeneities within the mixture. Furthermore, metals and other inorganic compounds can be found in waste streams as a result of the sorting and waste handling system. To simplify the estimations, in this work, all the blends studied are assumed to be free of organic additives, while the inorganic additives and impurities are treated as an inert mass of ash. Thus, only pure polymer compounds are considered for the feedstock composition. Fig. 2 shows the polymers that are most commonly found in waste mixtures, which are those used for the estimations and analysis throughout the present work.

In Fig. 2, Polyamide (PA), Polyurethane (PU) and Acrylonitrile Butadiene Styrene (ABS) describe families of polymers that can vary in structure, depending on the types of radical groups that are attached to their monomers (as, for instance, the family of Polyurethanes and Polyamides). In addition, there are co-monomers that are repeated a certain number of times in the same global monomeric structure (ABS for instance). However, the most commonly used polymers in the market or those with simpler structures are those selected to moderate the complexity of the blended system.

Here, a distinction is made between the natural rubber molecule (referred to in the *Results* section as 'NRubber'), which is mainly polyisoprene, and tire rubber (referred to as 'TRubber'), which is considered to comprise 71 % natural rubber and 28 % carbon black. Carbon black is included as a filler, and its percentage was selected based on the common composition of tires (see [29–32]).

In addition, Poly(methyl methacrylate) (PMMA; $C_5H_8O_2$, MW = 100.1 g/mol, LHV = 24.05 MJ/kg) and wool were considered. Wool's elemental balance was based on the typical composition of wool fiber [32].

2.2. Polymer classification and general cracking behavior

The polymers contained in the plastic waste are classified into three groups: aliphatic polymers, aromatic containing polymers, and heteroatom-containing polymers. These groups present characteristic behaviors under pyrolysis conditions.

2.2.1. Aliphatic polymers.

For common polyolefins such as polyethylene (PE) and polypropylene (PP), scission of the polymer typically occurs at random locations at low temperatures (>400 °C), which results in a blend of molecules with different lengths. At higher temperatures (e.g., 700–800 °C), the chain may break at the edges (end-chain scission), giving shorter molecules such as methane, while secondary reactions will be triggered leading to the generation of aromatics and polyaromatics [6,12,33].

Some polymers are more prone to yield monomers in a selective manner, e.g., those with large substituents along the main chain. For example, PMMA undergoes depolymerization or unzipping reactions, which can lead to recovery yields as high as 98 % [34].

2.2.2. Aromatic-containing polymers

In this group, aromatic rings may be derived directly from those already existing in the polymer structure, as in the case of polystyrene (PS) and PET, as well as copolymers that contain aromatic fractions, e.g., ABS. As an example, the rate of recovery of styrene from PS can reach up to 75 % at relatively low temperatures (i.e., 450 °C).

2.2.3. Heteroatom-containing polymers

Several widely used polymers contain heteroatoms in their structure

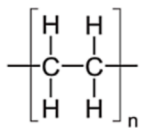
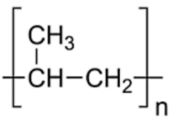
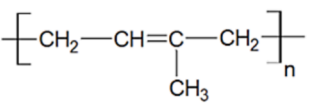
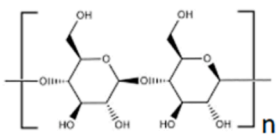
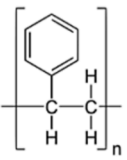
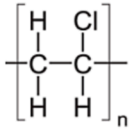
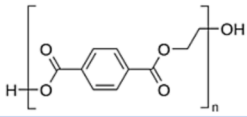
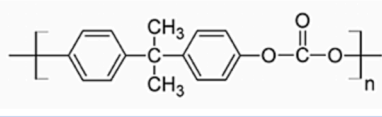
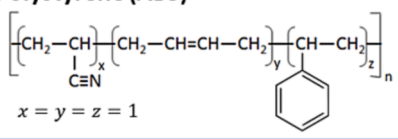
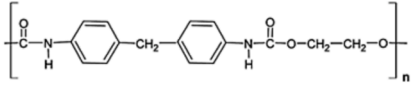
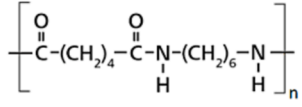
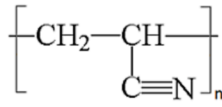
Polyethylene (PE) MF: C_2H_2 MW: 28.05 g/mol LHV: 42.8 MJ/kg 	Polypropylene (PP) MF: $(C_3H_6)_n$ MW: 42.08 g/mol LHV: 46.43 MJ/kg 	Polyisoprene (Rubber) MF: $(C_5H_8)_n$ MW: 68.12 g/mol LHV: 42.4 MJ/kg 
Cellulose (Cell) MF: $(C_6H_{10}O_5)_n$ MW: 162.14 g/mol LHV: 16.5 MJ/kg 	Polystyrene (PS) MF: $(C_8H_8)_n$ MW: 104.15 g/mol LHV: 41.9 MJ/kg 	Polyvinylchloride (PVC) MF: $(C_2H_3Cl)_n$ MW: 62.50 g/mol LHV: 22.9 MJ/kg 
Polyethylene-terephthalate (PET) MF: $(C_{10}H_8O_4)_n$ MW: 192.17 g/mol LHV: 22.9 MJ/kg 	Polycarbonate (PC) MF: $(C_{16}H_{14}O_3)_n$ MW: 254.28 g/mol LHV: 31.5 MJ/kg 	Acrylonitrile Butadiene Polystyrene (ABS) MF: $(C_{15}H_{17}N)_n$ MW: 211.31 g/mol LHV: 39.84 MJ/kg  <p>$x = y = z = 1$</p>
Polyurethane (PU) MF: $(C_{17}H_{16}N_2O_4)_n$ MW: 312.32 g/mol LHV: 21.8 MJ/kg 	Polyamide (PA) MF: $(C_{12}H_{22}N_2O_2)_n$ MW: 226.32 g/mol LHV: 30.7 MJ/kg 	Polyacrylonitrile (PAN) MF: $(C_3H_3N)_n$ MW: 53.06 g/mol LHV: 31.5 MJ/kg 

Fig. 2. Polymers commonly found in waste streams. MF, molecular formula; MW, molecular weight.

(e.g., oxygen, chlorine, fluorine, nitrogen). The heteroatoms may be part of the main chain bonds (e.g., PVC) or appear as side-branches (e.g., ABS). Heteroatoms can constitute highly reactive or weak bonds in the molecule [35]. These bonds can lead to preferred thermal decomposition paths that end up in recombination reactions or the generation of smaller and stable molecules, such as CO/CO₂, HCl, and NH₃. For instance, the elimination of carbon dioxide from carboxyl groups, water from hydroxyls, carboxylic acid from alkenoates, hydrogen chloride from chlorine attached to side or end-group chains, are typical products that are manifested in the thermal decomposition process [35–41].

Nitrogen-containing polymers, such as PU and PA, contain nitrogen in the inter-monomer bond, whereas polyacrylonitriles (PAN) contain nitrogen in the nitrile side-branch. Aliphatic PU and PA have relatively low thermal stabilities, as the amide and urethane linkages rearrange easily at temperatures in the range of 250°–450 °C. This rearrangement can lead to linear fragments that contain the functional groups of -amino (–CH₂–NH₂) and -nitrile (–CN), respectively, with the elimination of CO₂ and H₂O [40,41].

Oxygen-containing polymers such as aliphatic polyesters (e.g., PET) decompose in a similar fashion through an initial rearrangement of the ester linkage (–C=O–), which eventually splits out CO₂ if the severity of the operation is sufficient [37,38]. Cellulose (Cell) is a natural polymer with a high content of oxygen (O/C = 0.83), in the form of hydroxyl-side substituents and C–O–C bonds between the glucose monomers. The high oxygen content usually promotes the production of shorter oxygenated hydrocarbons fractions, which decompose further to produce CO and CO₂ [42].

Chloride-containing polymers, e.g., PVC, are known to lead to high levels of aromatization after the dehydrochlorination step [15]. The

high electronegativity of chlorine affects the electron density of the bond, thereby weakening the bond energy, as compared with C–C and C–H bonds. This makes the bond more-susceptible to breakage during a free-radical event, given that thermal scission is more likely to occur at locations along the chain where there are anomalies with respect to the electron density [35]. The chlorine located in alkyl chains will, when released, tend to remove a neighbor hydrogen to form hydrochloride, leaving behind a reactive site in the chain that can either react with other molecules present in the radical pool or form a double bond. The double bond formation event can lead to the creation of conjugated dienes that will act as precursors in the cyclization reaction [43], which will generate aromatic or polyaromatic structures.

In general, most of the polymers found in waste streams are fully decomposed to gas at around 500°–600 °C [33]. As the temperature increases beyond this range, further degradation occurs such that long chains are disintegrated to their simpler monomeric structures (C₂–C₄ and BTXS [benzene, toluene, xylene, styrene]), which are valuable for the intended chemical recycling in focus here. For olefinic polymers, this takes place in the temperature window of 600°–900 °C [12,33,34]. However, the higher temperatures can compromise the monomer yield and promote unwanted secondary cyclization reactions, which will end up in polyaromatic structures. In this work, the selected temperature was 800 °C, which represents a tradeoff between maintaining the total level of monomer recovery and the need to control harmful substances attributed to the presence of heteroatoms. For instance, previous experience has shown that the production of dioxins results from gas-phase or ash-induced reactions at high temperatures (>400 °C) [39,44], whereas at temperatures >800 °C, the levels of dioxins in the produced gas are drastically reduced [39,45,46]. Overall, in the present study,

organic molecules that contain heteroatoms were not considered as part of the product measurements, as they are present at low levels relative to their amounts at the selected temperature level [6,14,34,39]. Instead, the focus was on the hydrocarbon fraction and the carbon conversion slate of the cracking products.

3. Analysis method

3.1. Polymer blend estimation

Since each kind of polymer has a particular structure, the chain thermal decomposition profile of each polymer subjected to cracking conditions will also differ. Indeed, a specific blend of different polymers will have a defined product distribution under a given set of conditions. Therefore, to evaluate the correlations between the feedstock used and the product slate obtained from the cracking process, it is important to have knowledge regarding the polymer blend characterization.

To estimate the shares of the polymers in a particular feedstock blend, a system of equations can be formulated based on the elemental balances obtained from the ultimate analysis of the feedstock. In general, based on the mass conservation law, for a particular feedstock blend f , the mass fraction of element i will be the sum of the elemental contributions of all the polymeric compounds j present in the blend. Eq. (1) condenses this principle. The term E.N. refers to the Einstein notation of the summation expression and it will be used hereinafter in the matrix expressions.

$$\sum_j x_j^i a_{ji}^f = a_i^f \Rightarrow a_j^{i,f} x_j^f = a^{i,f} (E.N) \quad (1)$$

$$j \in \{PE, PP, PVC, \dots\}, i \in \{C, H, O, N, Cl, \dots\}$$

where a_j^i is the mass fraction of the element i in polymer j (units: kg_i/kg_j), x^j is the mass fraction of polymer j within the feedstock blend (units: kg_j/kg_f), and a^i is the mass fraction of element i in the feedstock (kg_i/kg_f). All quantities evaluated for a particular feedstock f . An additional equation can be formulated using the Low Heating Value (LHV) of the j component. Considering that enthalpy is a state function, the evaluation of the feedstock's LHV will depend on the initial and final states of its aggregated polymeric compounds. Therefore, it is reasonable to take the feedstock LHV as the weighted sum of the individual components, as presented in Eq. (2).

$$LHV_f x^f = LHV^f (E.N) \quad (2)$$

Finally, since the coefficient a^i corresponds to mass fractions, the mass conservation law for this set must be satisfied, as expressed in Eq. (3):

$$1_j x^f = m_{tot}^f (E.N) \quad (3)$$

where 1_j represents a $(1 \times j)$ vector of ones (covariant vector), and m_{tot}^f is the sum of the mass fractions of the element set evaluated (ideally, it should be equal to 1). The system constructed with Eqs. (1)–(3) can be regarded as a typical linear system of the form $Ax = b$, where x corresponds to the mass coefficient x^j , and A and b are defined by the stacked matrix and vector, respectively, as shown in Eq. (4):

$$A = \begin{bmatrix} a_j^i \\ LHV_j^f \\ 1_j \end{bmatrix}, b = \begin{bmatrix} a^{i,f} \\ LHV^f \\ m_{tot}^f \end{bmatrix} \quad (4)$$

From linear algebra theory, if the system $Ax = b$ is consistent (number of independent columns of A is equal to the set j size) and precisely determined (size of i set equal to size of the j set) it will have a unique solution.

When evaluating real physical systems, the target output vector b

will emerge from the results of the ultimate and proximate analyses of the feedstock. Then, the equations are transformed into inequalities that span the measurements' experimental uncertainty, and they will constitute the frame of the solution space. In the present case, x will be constrained by Eq. (5) and Eq. (6):

$$0 \leq x^j \leq 1, \forall j \quad (5)$$

$$|Ax - b| \leq \Delta b \quad (6)$$

where Δb corresponds to the error vector formed by the uncertainties of the elemental balance, the LHV and the total measured mass of the system (the latter is applied in those cases in which the system is not considered ash-free or not all the chemical elements are evaluated; the total mass fraction in those cases will be <1).

In the present case, the system is not always consistent or determined precisely. For instance, depending on the feedstock, the chemical/empirical formula for different polymers can be similar, or there may be more polymers in the blend than elements detected in the ultimate analysis, or *vice versa*. These scenarios create inconsistencies and unbalances in the matrix-based System, making the problem difficult to resolve and, in many cases, without a unique closed solution. To deal with this, a mathematical optimization procedure over a defined Loss function must be applied to obtain best estimates for the solution of the equation system.

While there is a wide variety of mathematical optimization techniques, all of them are rooted in the same principle: there is a transformation function with variable x that needs to be found, a set of constraints that limits the variable, and a defined Loss function that yields a real number that measures how far off the predictions of the estimated variable are with respect to the expected values of the transformation. Then, the optimization process consists of finding the value of x that minimizes the Loss function among the set of possible solutions that satisfy the constraints.

Convex optimization, which is a subset of the optimization problems family, deals with the problems that arise when the Loss function and the constraints are defined by convex functions. In general, these types of problems are defined in the form of the conditions set described in Eq. (7):

$$\begin{aligned} \text{Solve : } & \min_x L(x) \\ \text{Constrained by : } & g_l(x) \leq 0; \quad l = 0, 1, \dots, p \\ & h_u(x) = 0; \quad u = 0, 1, \dots, q \end{aligned} \quad (7)$$

with $L(x)$, $g_l(x)$, $h_u(x)$ satisfying the convex condition: $f(tx_1 + (1-t)x_2) \leq tf(x_1) + (1-t)f(x_2)$ with $f = L, g, h$, for $x_1, x_2 \in x \text{ domain}$

One of the common Loss functions used in convex optimization is defined by Eq. (8):

$$L(y) = y^T P y + c^T y + d \quad (8)$$

Eq. (8) corresponds to the general manner of a quadratic optimization. However, when the matrix P is a zero matrix, the problem is reduced to a linear optimization. For the concerned case, the Loss functions considered are defined as the sum squared error (Eq. (9)) and the fractional error of the matrix system (Eq. (10)), both of which can be derived from Eq. (8).

$$\begin{aligned} \text{Case 1 : } & y = Ax - b; \quad P = I, \quad c = 0, \quad d = 0 \\ \Rightarrow & L(x) = (Ax - b)_m (Ax - b)_m^m = \|Ax - b\|_2^2 \end{aligned} \quad (9)$$

$$\begin{aligned} \text{Case 2 : } & y = |Ax - b|; \quad P = 0, \quad c^n = \frac{1}{b^n} n, \quad d = c_m b^m \\ \Rightarrow & L(x) = c^T |Ax - b| = |c_i A_j^i x^j - d| \end{aligned} \quad (10)$$

where $\|\cdot\|_2$ is the Euclidean norm for a vector (or L2-norm). The constraints of the solution space will be defined by Eq. (5) and Eq. (6).

Various methods and algorithms have been developed to proceed with the optimization of the convex-constrained problems such as the one studied here and defined by Eq. (7) [47]. Specifically, first-order solvers, which are gradient-based methods, are robust and can be scaled to very large problems [48,49]. Here, two first-order solvers, Splitting Conic Solver (SCS) and Operator Splitting Quadratic Program (OSQP), were tested and implemented using a domain-specific language (DSL) called CVXPY, which can be used freely as a Python library under the Apache License. For more information about the solvers and the DSL used here, the reader is referred to the references for SCS [50,51], OSQP [52,53], and CVXPY [54,55].

3.2. Hyper-parameter optimization

The polymer compounds, the chemical elements, the Loss functions and the solvers form a set of conditions or hyper-parameters that control the final numerical approximation results. To avoid predefined or biased results, a grid searching technique [56] was applied to identify the hyper-parameter set that gives the best approximation under a defined metric. In this case, the metric was defined as the sum of the errors between the elemental balances and the LHV. The search was conducted for all possible combinations of the values that each condition could assume, as defined in Table 1.

Finally, the set of conditions with the lowest error in the metric was selected, to obtain the final estimated blend of the evaluated material (see Table 5 in Section 5). The selection was made with the prerequisite that all polymers from a composition based on prior knowledge (see Table 2) were included.

3.3. Bond-based characterization of feedstock and products

As a method to assess the correlation between the species obtained from the cracking process and the estimated polymeric compositions of the materials, a generalized classification approach to the chemical structure was implemented. The carbon product species were classified into the three most-relevant carbon compounds: CO_x, aliphatics, and aromatics. On the other side, the polymers in the waste material were evaluated based on a three-group categorization system for the carbons contained in its structure. These carbon groups were defined as: 1) carbons in a C-X bond, where X is a heteroatom of O, Cl, N, etc.; 2) carbons in an aliphatic bond (C-AL), which could be paraffinic or olefinic; and 3) carbons in an aromatic bond (C-AR), with only aromatic rings being counted here. The elemental mass fractions for the list of polymers presented in Section 2.1, as well as the carbon molar fractions for each of the three defined groups are presented in Fig. 3.

It is evident from the panels a and b in Fig. 3 that the chemical characteristics of the evaluated polymers are highly diverse. Going from the full aliphatic polymers (such as PE and PP) with the highest H/C ratios to the ring-based polymers (such as PS and PET) and the extensively heteroatom-substituted cellulose, the carbon-bonds spectrum of a waste stream is markedly heterogeneous. When a polymeric mixture enters the cracker, the organic synergies and the individual characteristics that may exist in the specific component set will be manifested. Then, the distribution of products from the cracking process must reflect these phenomena, which will depend on the feedstock blend

Table 1
Hyper-parameters set used to perform the tuning process.

Condition	Possible Values
Polymers	PE, PP, PVC, Cell, PS, PAN, PET, PA, PU, ABS, Nrubber, TRubber, PMMA, PC
Elements	C, H, Cl, O, N, S
Loss Functions	Sum_Squares, Fractional_Err
Solvers	SCS, OSQP

Table 2

Materials used in this work with their respective polymer compositions and general characteristics.

Material	Polymer Types	Chemical Characteristics	Description
Cardboard Recycling (CBR)	Polyethylene/ Polypropylene, Polyethylene Terephthalate (PET), Cellulose, Polyvinylchloride (PVC) (others: Polyurethane, Polyamide, Polystyrene)	- High aliphatic carbon content. - High oxygen content. - Medium ash content.	Post-consumer shredded stream of multilayer cardboard/plastic for food packaging. Form: Pellets
Cable Plastics (CP)	Polyethylene, Polypropylene, Polyvinylchloride (PVC). (Others: PET, Natural Rubber)	- High aliphatic carbon content. - High chlorine. - Rich in ash.	Non-separated waste from cable stripping. Only metals were sorted out previously. Form: Chopped pieces
Textiles (TXT)	Polyester (PET), Polyamide, Polyacrylonitrile, Cellulose (others: Wool, PVC, Polyurethane)	- Complex polymer blends. - Low aliphatic carbon content. - High heteroatom content.	Textile waste after sorting the useful pieces of cloth. Form: Pellets
Automotive Shredder Residue (ASR)	Polypropylene, Polystyrene, Polyurethane, Cellulose, PVC (others: Tires Rubber, Acrylonitrile Butadiene Styrene (ABS), Polycarbonate (PC), PE, Polyacrylonitrile, PMMA)	- Low polyolefin content. - High aromatic. - Rich in heteroatoms. - Rich in ash.	Shredder Residue (SR) from the automotive and electrical waste (WEEE) sorting. Form: Pellets

characteristics.

4. Experimental setup and materials

The experiments for the present work were performed in the 12-MW_{th} CFB boiler with an integrated – MW_{th} BFB gasifier/cracker, together forming a pilot-scale DFB system (see Fig. 4). The installations serve as the heat production unit for the Chalmers campus. The boiler in the CFB unit, is fed with wood chips using a hopper and a system of conveyor belts. The fluidized bed material is collected by a cyclone and directed to the BFB reactor via a particle distributor and a loop seal. Thereafter the bed material returns to the boiler via another loop seal. The BFB reactor and both loop seals are fluidized with steam to keep the reaction environment oxygen-free. As a whole, the DFB system runs with around 3 tons of bed material, which acts as a heat transfer medium between the CFB and the BFB cracker reactors. The polymer-rich feedstock for the tests is fed at a rate that can vary from 30 to 300 kg/h and can enter into the cracker at two alternative positions, either at the top of loop seal 1 (marked as 6 in Fig. 4) or at the cracker fuel input point (marked as 8 in Fig. 4). The feeding system at point 6 consists of an extruder where the feedstock in pellets or granulate form is compressed and heated to get a molten flow that pours down on the bed material. In contrast, if the feeding occurs at point 8, the feedstock is fed as pellets or granulates by gravity on to the bed material of the cracker reactor via a set of rotary valves working as an airlock system. A detailed description of this system can be found in reference [57]. The cracker conditions and the feeding points used for each of the tested materials are reported in Table 4.

As shown in the DFB schematic of Fig. 4, the gas produced from the cracking is combusted in the boiler after taking a sample stream for analysis purposes. In general, both the flue gas and the raw gas are analyzed continuously during trials. The complete sampling system is

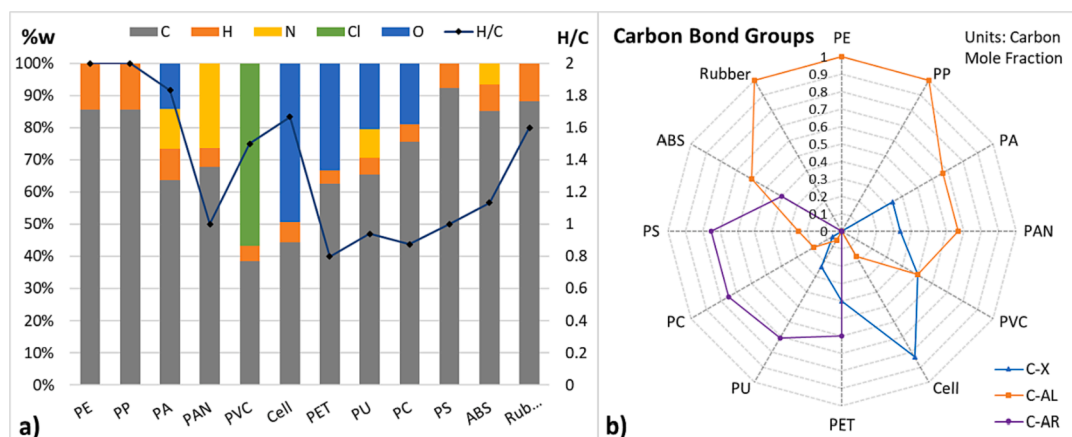


Fig. 3. Chemical characteristics of polymers commonly found in plastic waste streams. Panel a, Elemental compositions and H/C ratios. Panel b, Carbon mole fractions of the polymers according to the three defined bond groups (X refers to a heteroatom of oxygen, nitrogen and chloride, AL: aliphatic, AR: aromatic).

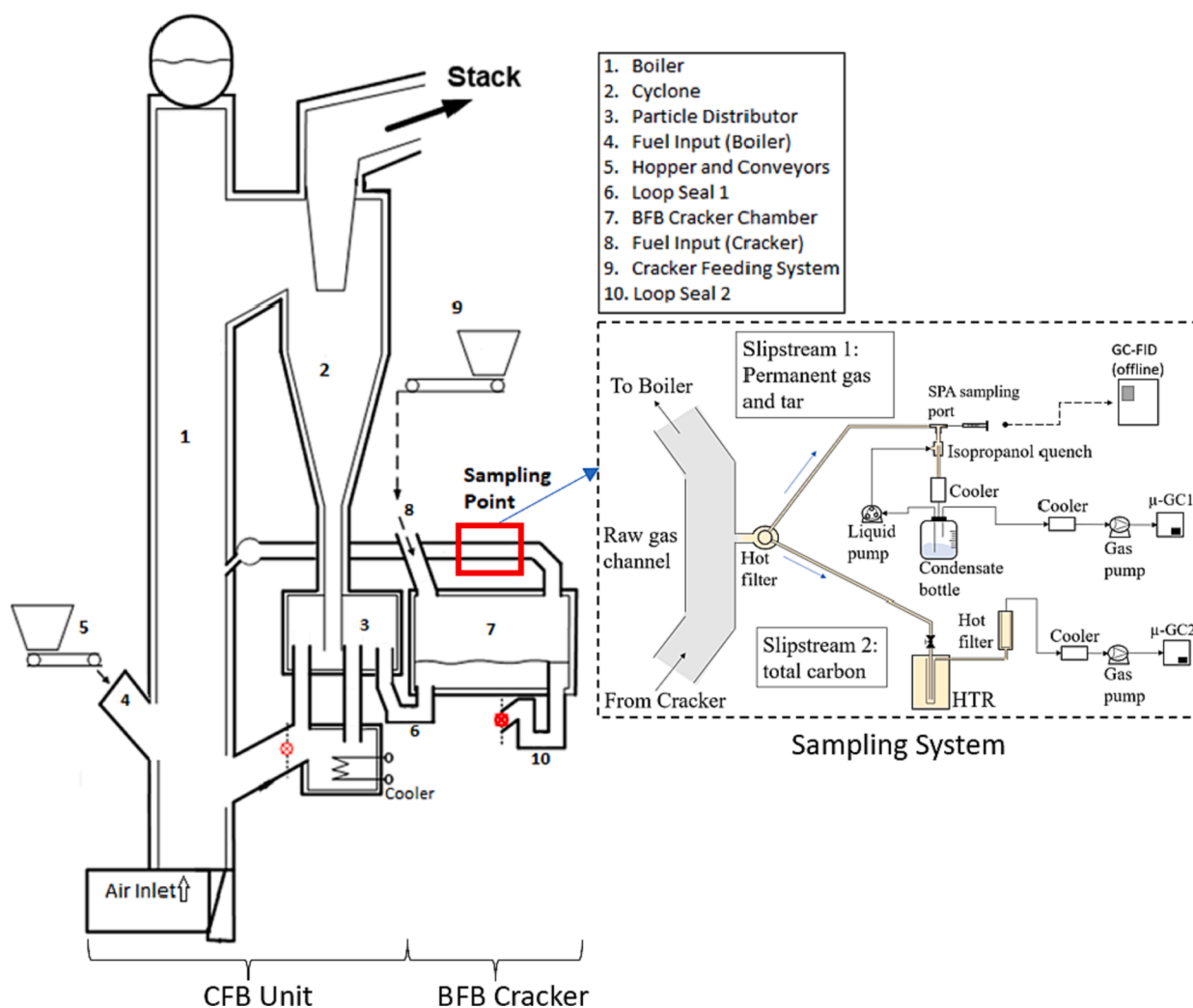


Fig. 4. Schematic of the Chalmers DFB plant used in this work (modified from [58]).

depicted on the right-hand side of Fig. 4, and described below.

The sample is extracted from the raw gas channel and pass through a hot ceramic filter (350 °C) where the sampling stream is split in two. One slipstream is dedicated for permanent gases, aliphatics and aromatics characterization (Slipstream 1 in Fig. 4), whereas the other slipstream is

dedicated to total carbon characterization (Slipstream 2) with the help of a High Temperature Reactor (HTR). In Slipstream 1, the aromatics and condensable species are captured using a Solid-Phase Adsorption (SPA) method before any cooling takes place. The remaining gas in the slipstream passes through an isopropanol quenching system with further

cooling to get a dry gas stream that is pumped to a Varian CP-4900 micro-GC (μ -GC1) coupled to a Thermal Conductivity Detector (TCD). On the other hand, the aromatics are characterized offline in a Bruker GC430 GC coupled to a flame ionization detector (FID). In the Slipstream 2 the hot gases are sent for full reforming at 1700 °C in the HTR, to later be characterized in another micro-GC (μ -GC2). Due to the large diversity of species formed in the cracking process, this slipstream's purpose is to measure the total carbon in the cracking gas and be able to estimate by difference the char or soot that remain in the cracker as well as the contribution of the unmeasured species to the carbon balance (see Fig. 5). The expected unmeasured species in the sampling gas are C4 and larger aliphatic along with other unidentified aromatic species. In general, the reported measurements correspond with averages taken over 25 to 30 min of continuous sampling to the micro-GCs (eight to ten chromatograms) and taking four SPA samples per material. Given the intrinsic fluctuations of the process at the tested scale, as a threshold rule for the data quality assessment, the maximum allowed standard deviation was 10 %.

As a summary, the species quantified, and the characterization techniques used in the present work are summarized in Fig. 5. For more information about this sampling setup, see reference [58,59].

4.1. Materials and cracking conditions

Considering the range of polymeric waste materials from highly sorted fractions to highly blended residues, a general recycling method such as thermal cracking becomes an option if the material cannot: a) be recycled with reasonable separation and sorting efforts; or b) be recycled into high-quality materials. Four representative mixed materials were used as feedstocks for the cracking process in this work: Reject from Cardboard Recycling (CRB); Cable Plastics (CP); Textiles (TXT); and Automotive Shredder Residue (ASR). All four materials have in common that they are residues from post-consumer recycled products. The different polymers contained in each material are presented in Table 2. Since the exact shares of these species in the blend are unknown, they are estimated using the methods presented in Section 3.1. The materials classified as "others" (within parentheses), are taken as optional in the numerical blend estimation.

The elemental balances derived from the ultimate analysis performed on each material are presented in Table 3. In the case of ASR, two different batches with different elemental compositions (resulting from different rejection processes) were analyzed.

The main operational conditions for the BFB cracking reactor are indicated in Table 4. The temperature range was $800^\circ \pm 10^\circ \text{C}$ and the bed material circulation was around 15 tonnes/h. The BFB cracker was fluidized with steam and the fuel residence time was estimated to be around 4–5 min, and the gas residence time was 5–10 s. The main difference between the trials was the type of bed material used: olivine was used for the ASR, while silica sand was used for the CRB, CP and TXT.

Pure polyethylene (PE) was also included in the analysis, for comparison purposes.

5. Results and analysis

5.1. Results of the thermal-cracking process

Fig. 6 shows the compiled results from the thermal cracking experiments performed under the conditions described in Section 4.1 for the evaluated materials (see Table 4). For the relevant group species presented, the lowest and highest values of the uncertainties obtained across all the evaluated materials were $\text{CO} + \text{CO}_2 = 1\text{--}3\%$, $\text{C}_2 + \text{C}_3$ monomers = $1\text{--}3\%$ and $\text{BTXS} = 1\text{--}4\%$; for the rest of the species and groups presented the uncertainties were lower than 5 %.

In Fig. 6, the product distributions of the different materials display different behaviors when subjected to the thermal-cracking conditions. Compared with PE, all the materials display a decrease in the total aliphatic yield, which is expected given their heterogeneous compositions. The CO_2 production levels are significantly high ($> 0.30\text{kg/kgf}$) for all the materials, with the exception of CP, the CO_2 level of which is similar to that for PE ($< 0.10\text{kg/kgf}$).

The level of production of olefin monomers (C_2 and C_3) per kilogram of material is highest for CRB and lowest for TXT, according to the following order: $\text{CRB} > \text{CP} > \text{ASR} > \text{TXT}$. Conversely, the production of aromatic monomers (i.e., BTXS) is highest for TXT, with levels comparative to those for PE, and lowest for ASR, in the following order: $\text{TXT} > \text{CRB} > \text{CP} > \text{ASR}$. CRB and CP showed similar yields of BTXS. Overall, total monomeric production (olefins + BTXS) per kilogram of material is $< 55\%$ of the PE levels (0.54kg/kgf), and a decreasing trend is observed in the order of: $\text{CRB} > \text{CP} > \text{TXT} > \text{ASR}$, until the production level reached 14 % for ASR.

In the case of methane, a decreasing trend (albeit not as steep) is observed for the same sequence, with CRB and CP yielding levels similar to those yielded by PE ($> 0.1\text{kg/kgf}$) and falling by around 70 % (to 0.03kg/kgf) for TXT and ASR. In contrast, the char levels show an increasing trend with the opposite sequence as the total monomeric yield, with the lowest level reported for CRB at 0.042kg/kgf , which was similar to that of PE, and increasing 4-fold to the highest level at 0.18kg/kgf for ASR.

In terms of the effectiveness of the carbon conversion process for each material, Fig. 7 presents the carbon percentages with respect to the carbon contents of the materials (Table 3). Similar trends are observed across all the materials, as shown in Fig. 6.

In terms of monomer recovery, two levels of olefin monomers ($\text{C}_2 + \text{C}_3$) can be observed in Fig. 7. For CRB and CP, the carbon conversion rate is close to 30 %, while for TXT and ASR it is $\leq 10\%$. The difference in the conversion to BTXS is not so wide between the materials, ranging from 16% for TXT to 8% for ASR. In general, the total rate of carbon conversion to monomers is around 40 % for the CRB and CP materials (44 % and 38 %, respectively), which is close to the PE value (60 %), and then it falls by 41 % to the TXT and ASR levels (20 %).

The rate of carbon conversion to CO_x is $> 24\%$ (CRB) for most of the materials until it reaches 33 % for ASR, with the exception of CP, which shows a carbon conversion rate of around 6%, which is similar to that for PE (4%). The percentage CO_2 emissions range from 15 % for CRB to 26 % for ASR (60 % to 78 % of the total CO_x released), and for CP it is 3 %.

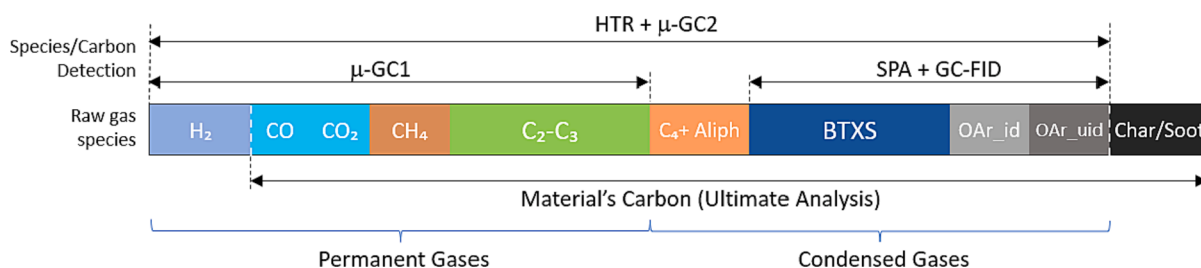


Fig. 5. Quantified raw gas species and characterization methods. (BTXS: Benzene, Toluene, Xylenes and Styrene, OAr-id: Other identified aromatics, OAr-uid: Other unidentified aromatics).

Table 3Elemental compositions in %w_{dry} and respective errors (%Er) of the materials analyzed in the present work (d: dry basis).

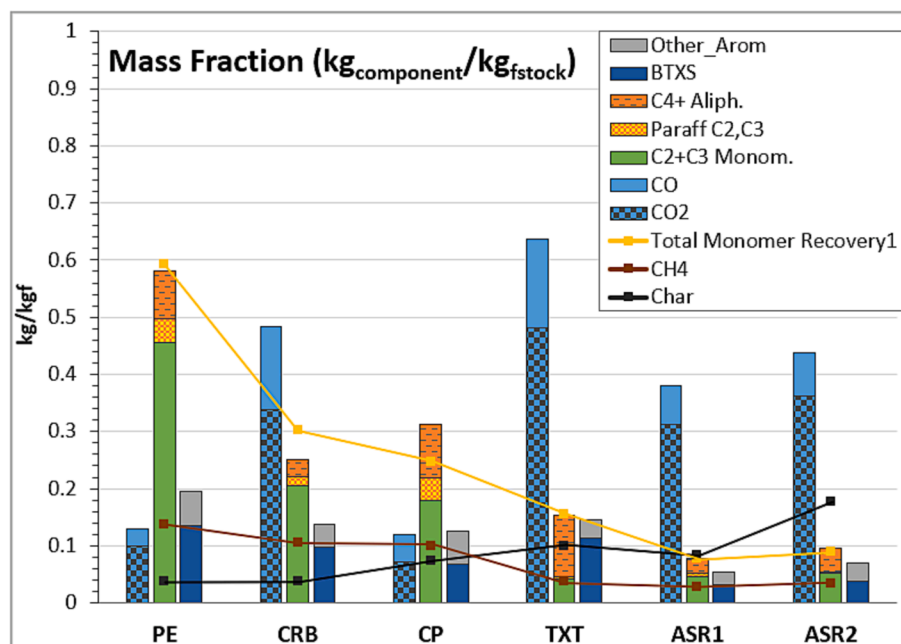
Element	CRB		CP		TXT		ASR 1		ASR 2	
	%w _d	%Er	%w _d	%Er	%w _d	%Er	%w _d	%Er	%w _d	%Er
C	60.60	5.0	57.00	2.0	60.53	5.0	33.00	5.0	47.00	5.0
H	9.00	13.0	8.50	6.0	5.17	5.0	4.20	13.0	5.40	13.0
O*	21.00	15.5	0.66	12.5	29.97	5.0	13.66	10.7	13.17	10.7
N	0.35	29.0	0.02	6.0	2.90	6.0	1.30	29.0	1.60	29.0
S	0.07	10.0	0.02	6.0	0.09	9.1	0.33	10.0	0.19	10.0
Cl	0.20	25.0	5.80	6.0	0.12	7.6	0.51	25.0	0.64	25.0
Ash	8.75	11.0	28.00	3.0	1.22	15.9	47.00	11.0	32.00	11.0
LHV(MJ/kg)	30.14	5.0	27.20	7.2	28.13	7.4	13.90	15.0	20.10	15.0

* calculated by difference.

Table 4

Main operational conditions for the BFB cracking reactor.

	PE	CRB	TXT	CP	ASR 1	ASR 2
Temperature Cracker	800	805 °C	800 °C	800 °C	790 °C	790 °C
Bed material	Silica Sand	Silica Sand	Silica sand	Silica sand	Olivine	Olivine
Steam Flow (kg/h)	120	45	150	130	160	160
Material Flow (kg _{daf} /h)	90	40	150	108	159	157
Feeding Mode	Molten flow via extrusion	Molten flow via extrusion	Top Feeding by gravity	Top Feeding by gravity	Top Feeding by gravity	Top Feeding by gravity
Feeding Position	6	6	8	8	8	8
Steam/Fuel ratio	1.3	1.1	1.0	1.2	1.0	1.0

**Fig. 6.** Results of the cracking DFB process for the evaluated materials in terms of mass ratio (kg/kgf).

Methane production accounts for equal carbon levels for CRB and CP (13.1%) and drops 43 % to the TXT and ASR levels, which have carbon conversion rates of 4.8 % and 6 % respectively.

The production levels of other aliphatics, such as paraffins C2 and C3 and long-chain C4+ aliphatics, are highly variable across the different materials, with the highest levels reported for CP and TXT at around 20 %, and the lowest for CRB and ASR at 7 %. C4+ aliphatics represent the largest share among the other aliphatics set ranging between 65 % and 98 % for the group, which correspond respectively with 6.5 % for CRB at the lowest and 18 % for TXT at the highest carbon conversion ratio. Paraffins C2 and C3 vary greatly, with the highest carbon conversion ratio at 5.6 % for CP and the lowest at 0.4 % for TXT.

For aromatics other than BTXS, which includes the polyaromatics set, similar levels of carbon conversion as were seen for PE are obtained for CRB and ASR (at around 6 %). In this set, the highest level is for CP at 9 % and the lowest level is for TXT at 4.6 %.

Carbon conversion to char spans a wide range and increases between materials as their total monomer recovery is reduced, albeit with a steeper trend on average. Starting from CRB at 6.4 %, the conversion rate extends beyond the 25 % level to reach 37 % for ASR.

5.1.1. Material composition estimations

After applying the hyper-parameter optimization described in

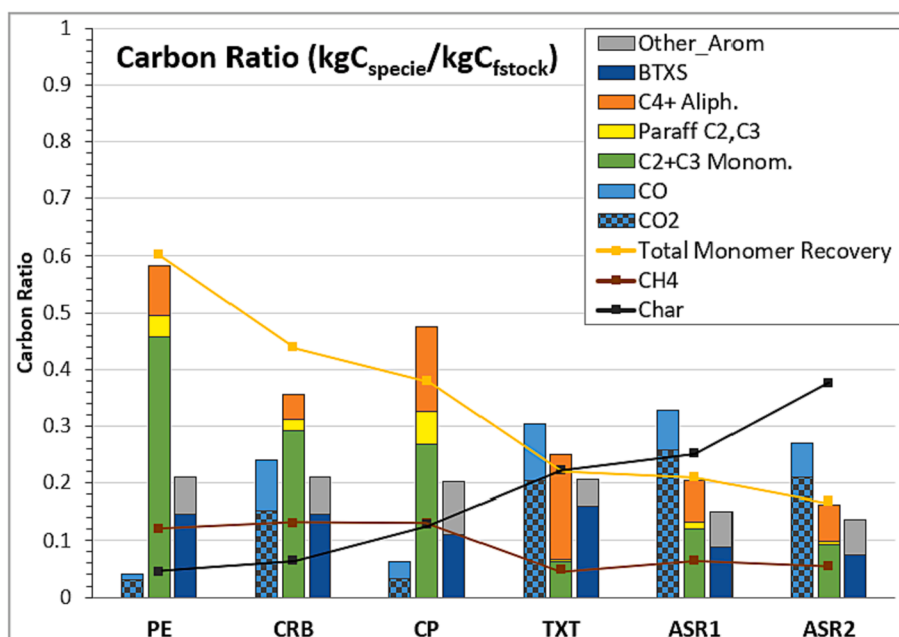


Fig. 7. Results of the cracking DFB process for the evaluated materials in terms of the carbon ratio.

section 3.2 to the evaluated materials, and based on the elemental information in Table 3, the results of the estimated polymer composition are presented in Table 5. The pure PE feedstock used as reference case in this work is included as an example for the table interpretation.

Table 6 presents the averaged values of the residuals for each of the balances considered in the equation system. The Columns “E_err%” and “LHV_Err%” correspond respectively to the sum of the relative error between the estimated and the expected values for all the elements considered and the relative error for the LHV.

From Table 6, it is evident that the optimizations have a good degree of approximation, with a low total error for the elemental balance. The averaged LHV error is lower than 10 % in all the cases, except for TXT, which has an LHV error of 17 %. This is acceptable considering the pure components approximation used here, whereby other small fraction polymers or additives are considered to be negligible. For the elemental balance, the error is low for most of the materials. The relatively large error presented in some of the cases, e.g., CP, is due to a very low weight share of some of their elements (N and O for CP). However, in reality, the approximation is very good despite these low elemental levels, as can be observed in the residual values shown in Table 6.

While both solvers (SCS, OQPS) gave similar results when evaluated with the same Loss function, the more-stable solver was SCS. Regarding the Loss function, the best one was the Fractional Error metric of Equation (10), corresponding to a linear optimization, which is in line with the linear nature of the evaluated problem.

In general, the numerical estimation performed for the various materials give results that are within the expected ranges for each polymer component, based on a visual pre-identification of the material, common material production composition, and/or rough elemental estimations. Cases close to the limits, such as PP in ASR, are probably due to some plastic pre-selection performed on-site before the rejection, which could affect the polymer distribution through assigning lower concentrations to certain components than others. Fig. 8 presents the mass fractions (in kg/kg_{daf}, daf: dried ash free feedstock) of the different polymers in the evaluated materials.

5.1.2. Correlation of material cracking conversion and composition

The carbon atoms of the polymeric components were grouped based on their bond type, according to the classification presented in Section 3.3, and summed correspondingly with their respective estimated shares

for each material (Table 5). Here, the C-X group is split into C—O (carbons with an oxygen atom attached) and C-Xh (carbons with another heteroatom attached). For cases in which a carbon was attached to more than one type of heteroatom, priority was given to oxygen, due to it having a higher likelihood to form products with carbon, e.g., CO and CO₂, at the end of the process. With this classification, the resulting evaluation is shown in Fig. 9 (panel a) for each of the original feedstock materials in terms of their carbon ratios (based on the material's carbon content, listed in Table 3). Fig. 9 (panel b) presents the carbon ratios of the respective thermal-cracking yields (converted from the kg/kgf of Fig. 6) and grouped based on the same carbon classification.

In Fig. 9, it is possible to observe the variation of the different carbon groups when the materials are subjected to cracking conditions. The polymer composition estimation of Table 5, in combination with knowledge of the cracking products, opens the door to understanding some key outcomes of the carbon conversion that took place within the process. Considering the C-X groups, from Fig. 3, the main contributors to these groups are Cell, PET, PA and PVC. From these, the first two compounds contain significant amounts of oxygen in terms of weight, and they are the main contributors of C—O carbons (see Fig. 3, panel b), which is attributed to the CRB, TXT and ASR materials having a large proportion of C—O in their structures (see Fig. 9, panel a). This is reflected also in the large amounts of CO_x obtained from the conversion process compared with the levels obtained from the conversion of CP, which has no C—O in its structure.

Since the CO_x levels are lower than the levels of C—O for CRB and TXT, this means that part of the carbon in the C—O bonds is converted into species other than CO_x, such as aliphatics, aromatics/polyaromatics or char. Those materials contain polymers in which oxygens are shared between two carbons in an ether or ester linkage, as in for instance Cell and PET. An example of this is TXT, which is mostly PET, which has no C-AL according to the classification rules due to the ester linkages to the only two aliphatic carbons of the monomeric structure. In this material, the total amount of C-AL is low (14 %) but after the conversion, the reported aliphatic species was doubled, mostly being C4+ aliphatics. Although half of the aromatics in this material were converted to char, indicating a significant activity of secondary reactions (also evidenced by the large C4+ aliphatics share), they maintained more or less the same C-AR levels, indicating that either all the carbons in C-AR remained as carbons within a ring or that the total balance in the inter-

Table 5

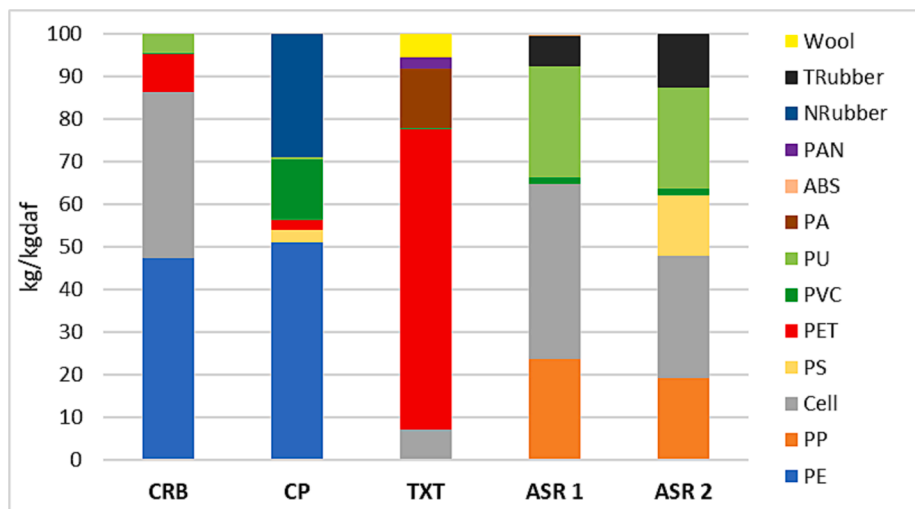
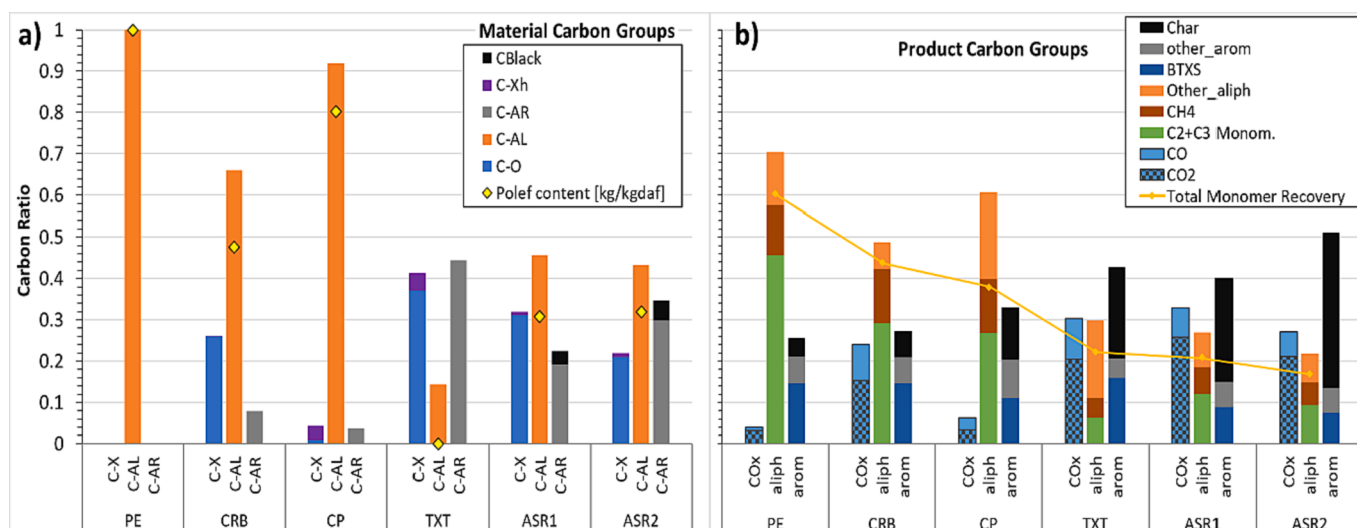
Estimations of the polymeric compositions for each material. (in the table: Polef = PE + PP + Rubber. Other alloys include ABS, PC, PMMA and other polymeric compounds not evaluated here).

	Solver	L. Function	PE	PP	Cell	PS	PET	PVC	PU	PA	ABS	PAN	NRubber	TRubber	Wool	PC
PE	<i>Expected (kg/kgdaf)</i>		100													
CRB	SCS	Fract_Err	43.40		35.64		7.85	0.36	3.90							
	SCS	Fract_Err	43.40	<0.01	35.64		7.85	0.36	3.90							
	OSQP	Sum_Sqr	42.97	<0.01	35.23	<0.01	8.24	0.36	4.34	<0.01						
	<i>Average (kg/kgf)</i>		43.25	<0.01	35.50	<0.01	7.98	0.36	4.05	<0.01						
	<i>Estimated (kg/kgdaf)</i>		47.40	<0.01	38.91	<0.01	8.75	0.40	4.44	<0.01						
	<i>Expected (kg/kgdaf)</i>		PE + PP >40		<50		5–12	<1	PU + PA + PS <5							
CP	SCS	Fract_Err	36.71	<0.01	<0.01	1.92	1.84	10.22	0.22				21.06			
	SCS	Fract_Err	36.37		<0.01	1.71	1.84	10.22	0.22				21.61			
	SCS	Fract_Err	37.24	<0.01		2.25	1.84	10.22	0.22				20.20			
	<i>Average (kg/kgf)</i>		36.78	<0.01	<0.01	1.96	1.84	10.22	0.22				20.95			
	<i>Estimated (kg/kgdaf)</i>		51.08	<0.01	<0.01	2.72	2.56	14.20	0.31				29.10			
	<i>Expected (kg/kgdaf)</i>		Polef >70					>10	PU + PA + PS <2				Polef			
TXT	SCS	Fract_Err			7.08		69.42	0.22	<0.01	13.85		2.60			5.62	
	SCS	Fract_Err			7.11		69.44	0.22		13.83		2.64			5.54	
	OSQP	Fract_Err			7.06		69.59	0.22	<0.01	13.55		2.74			5.63	
	<i>Average (kg/kgf)</i>				7.08		69.48	0.22	<0.01	13.74		2.66			5.60	
	<i>Estimated (kg/kgdaf)</i>				7.17		70.34	0.22	<0.01	13.91		2.69			5.67	
	<i>Expected (kg/kgdaf)</i>				<15		>60	<1	PU + PA + PAN >10 and <20						< 10	
ASR 1	SCS	Fract_Err		12.51	21.75	<0.01		0.90	13.67		<0.01	<0.01		3.84	<0.01	
	SCS	Fract_Err		12.51	21.75		<0.01	0.90	13.67		<0.01			3.84		
	SCS	Fract_Err		12.51	21.75		<0.01	0.90	13.67					3.84		<0.01
	<i>Average (kg/kgf)</i>			12.51	21.75	<0.01	<0.01	0.90	13.67		<0.01	<0.01		3.84	<0.01	<0.01
	<i>Estimated (kg/kgdaf)</i>			23.60	41.04	<0.01	<0.01	1.70	25.80		<0.01	<0.01		7.24	<0.01	<0.01
	<i>Expected (kg/kgdaf)</i>		PP >20, Polef >30		>10			<2	PU + PA + PS >20		Other alloys <10			Polef >30		
ASR 2	SCS	Fract_Err		13.13	19.47	9.60		1.13	16.00	<0.01	<0.01	<0.01		8.67		<0.01
	SCS	Fract_Err		13.07	19.48	9.66		1.13	15.98			<0.01		8.68		<0.01
	SCS	Fract_Err		13.03	19.48	9.70		1.13	15.98					8.68		
	<i>Average (kg/kgf)</i>			13.08	19.48	9.65		1.13	15.99	<0.01	<0.01	<0.01		8.68		<0.01
	<i>Estimated (kg/kgdaf)</i>			19.23	28.64	14.20		1.66	23.51	<0.01	<0.01	<0.01		12.76		<0.01
	<i>Expected (kg/kgdaf)</i>		PP >20, Polef >30		>10			<2	PU + PA + PS >20		Other alloys <5–10			Polef >30		

Table 6

Residuals of the calculations (averaged).

Material	C	H	O	N	S	Cl	m_tot	LHV	E_err %	LHV_err%
CRB	-5.49E-05	-1.59E-04	4.81E-05	1.31E-04	0.00E+00	6.90E-06	-2.71E-05	-2.97E+00	1.86	9.59
CP	-1.55E-07	1.35E-06	-6.05E-08	3.86E-07	0.00E+00	-1.44E-07	-1.38E-06	-1.69E+00	0.21	6.23
TXT	1.71E-05	-2.93E-05	5.69E-06	-4.78E-06	-4.48E-06	7.20E-06	-8.54E-06	-4.78E+00	1.61	16.97
ASR 1	-8.43E-04	3.22E-08	-1.83E-07	4.56E-10	0.00E+00	4.01E-08	-4.92E-07	-1.23E-01	0.26	0.88
ASR 2	4.79E-06	-2.32E-05	2.35E-06	5.40E-06	6.14E-06	2.12E-06	-2.41E-06	-3.26E-01	0.54	1.62

**Fig. 8.** Estimated polymeric compositions (mass fractions) in kg/kgdaf for the evaluated materials.**Fig. 9.** Carbon ratios of each material's composition before (panel a) and after (panel b) the thermal-cracking conversion. The carbons are classified into three groups: C-X, C-AL and C-AR groups for the original material composition; and COx, aliphatics and aromatics for the cracking products.

group conversion to aromatics was close to zero. Thus, the only significant contributions to aliphatic species in relation to the original group levels came from C-X, and mainly C—O. For ASR, the opposite is true. Even though the oxygen content of ASR is lower than that of TXT, the share of COx after the cracking is higher. This can be explained by the ash-induced effect of oxygen transport through the circulation of solids in the DFB system, as described in detail by Pissot et al.[60].

Regarding the aliphatics bond group (C-AL), polyolefins such as PE, PP and Rubber are the main contributors to this group (See Fig. 3 and Section 3.3). Thus, the highest C-AL levels are obtained for those materials that have a high polyolefinic share, such as CRB and CP (Polefins:

47 % and 80 %, respectively). Those materials with high numbers of linear aliphatic bonds, such as CRB and CP, are the ones with the highest levels of olefin-monomer recovery, reaching values close to those seen for PE. Even between ASR and TXT it is possible to observe from Fig. 8 that the former has a larger content of linear polyolefins, which is reflected in a relatively higher olefin-monomer conversion than in the latter case.

As pointed out previously, the aromatics formation rate is similar for all the materials, even though they have different compositions. Two mechanisms were described in Section 2 as the main contributors to aromatics formation: 1) the thermal decomposition of polymers that

contain aromatic structures; and 2) the aromatization by cyclization of precursors from the cracking reactions. The first mechanism often yields monoaromatics, which is why TXT presented with the highest conversion to BTXS (16 %), since its dominant share is for PET, which is a major reservoir of aromatic structures (see Fig. 3). The second mechanism is the formation path followed by the high-polyolefinic materials such as PE, CRB and CP, which despite the lack of aromatic groups in their structures yielded total aromatics fractions similar to those of TXT, through cyclization reactions. However, this path, if not controlled, will lead to the formation of polyaromatics. Indeed, the BTXS fractions of the aforementioned high-polyolefin materials are smaller than that for TXT. Relative to the production of aromatics (char excluded), the BTXS share was the highest at 91 % for TXT, followed by CRB with 70 % (same as PE), then ASR at around 57 % and finishing with the lowest level for CP at 54 %. Again here, the lack of polyaromatics in TXT is an indication that the yielded BTXS species are predominantly a product of decomposition rather than aromatization.

On the other hand, it is worth noting that CP has the lowest BTXS fraction with respect to the aromatics group across all the materials, and even has a lower carbon share of olefin monomers than CRB. Nonetheless, its linear polyolefin content is the highest among all the materials. Here, the effects of the secondary reactions in the products released from the cracking process are manifested. As explained in Section 2.2, chloride-containing components, particularly PVC, are known to lead to high levels of aromatization in the de-chlorination process, due to an increased odds of generating double bond formation and conjugated dienes that act as precursors in cyclization reactions. In addition, hydrochloride is a contributor to cyclization reactions via the Diels-Alder reactions between olefins of the nascent cracking volatiles, towards the formation of aromatic and polyaromatic structures [43]. This is also evidenced by the reduced carbon share of olefin monomers of CP with respect to the CB and PE cases, since ethylene and propylene in particular are known to act as good dienophiles in the cyclization reactions.

Regarding the char formed during the thermal cracking, the polyolefin-rich materials, such as CRB and CP, gave relatively limited levels of char production, at 6 % and 13 %, respectively. In contrast, TXT and ASR gave higher yields of char, which included not only the char formed from the polymeric composition but also eventual soot formed from excessive aromatization and the carbon-based fillers (carbon black). The formed char exits the cracking zone together with the sand to enter the combustor, thereby contributing to heat production. Alternatively, it is filtered out from the raw gas. It should be noted that in the DFB system used, the combustor is a full-scale boiler running on biomass at all times and the amount of char formed does not have an effect on the

overall heat balance of the DFB system.

Bidimensional pair-plotting was performed (Fig. 10) to determine the cross-correlations between the input feedstocks and cracking products according to the defined carbon bond group classification. The x-axis in Fig. 10 corresponds to the feedstocks' carbon fractions of C—O, C-AL and C-AR (panels a, b and c, respectively), while the y-axis represents the products' carbon conversion of the evaluated carbon species in each plot.

The correlations between the input carbon bond groups and the cracking products are revealed. From Fig. 10a, it is clear that COx is positively and apparently linearly correlated with the C—O carbons (blue markers in plot a). As expected, the linear trend starts above the diagonal (at COx = 0.05 for PE), given the immanent oxygen presence in the process due to the steam environment. The same positive correlation is observed in Fig. 9c for COx with the aromatic bonded carbons (C-AR). Conversely, in Fig. 10b, there is an overall negative correlation with the aliphatic bonded carbons (C-AL), which is linked to the decreasing level of oxygen in the feedstock as C-AL is increasing, where COx stays at about 0.3 for a C-AL level <0.5, and then starts to decline to reach the level for pure PE (0.05).

In Fig. 10b, aliphatics show a positive correlation with C-AL (orange markers in plot b) as expected, while in Fig. 10a there is a negative correlation with C—O, which chemically has a stronger tendency to end up as a COx species. The correlation of aliphatics with C-AR is also negative, which indicates a low chance that the rings open and yield linear structures. Aromatics (gray markers) present slightly positive correlations with C-AR and with C—O (Fig. 10c and Fig. 10a, respectively), while they have negative correlations with C-AL (Fig. 10b), although it does not end up at or close to zero, indicating the unavoidable generation of ring structures even when the original molecule has no such structures.

Deviations from apparent linearity in all the plots is observed for TXT. This is probably due to the low content of polyolefins, as shown in Fig. 9, and the phenomenon whereby other groups, especially C—O, are converted into aliphatic species at the end of the cracking process. These characteristics of TXT cause it to behave as the extreme case for all the plots in Fig. 10.

Specific individual species and groups of species can be plotted in the same way as in Fig. 10 to evaluate potential correlations with the carbon bond-based characteristics of the incoming feedstock. In the concerned case, the olefin C2, C3 monomers and BTXS are plotted against C-AL and C-AR in Fig. 11. Methane is also included for illustration purposes.

In relation to monomer recovery, it is evident from Fig. 11a and b, that there are relatively well-defined quasi-parabolic trends for the case

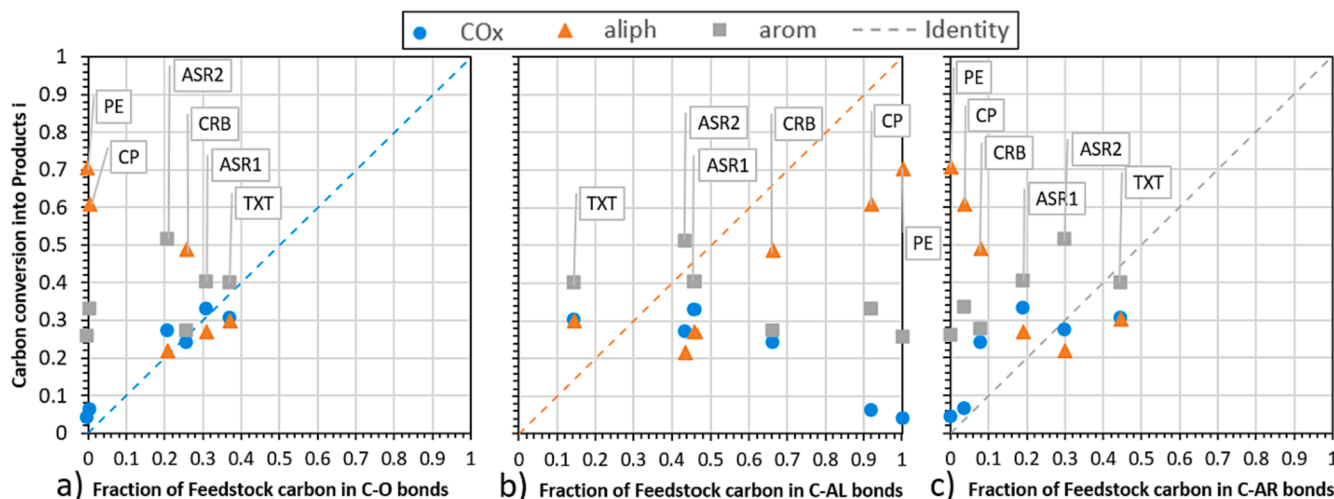


Fig. 10. Carbon conversion into product compound *i* (kgC of species *i* in product per kgC in feedstock) as a function of the fraction of the carbon bond group *j* in the feedstock (kgC in bond type *j* per kgC in feedstock). Carbon Bond group *j* = C-O, C-AL, C-AR; product compound *i* = COx, aliph, arom.

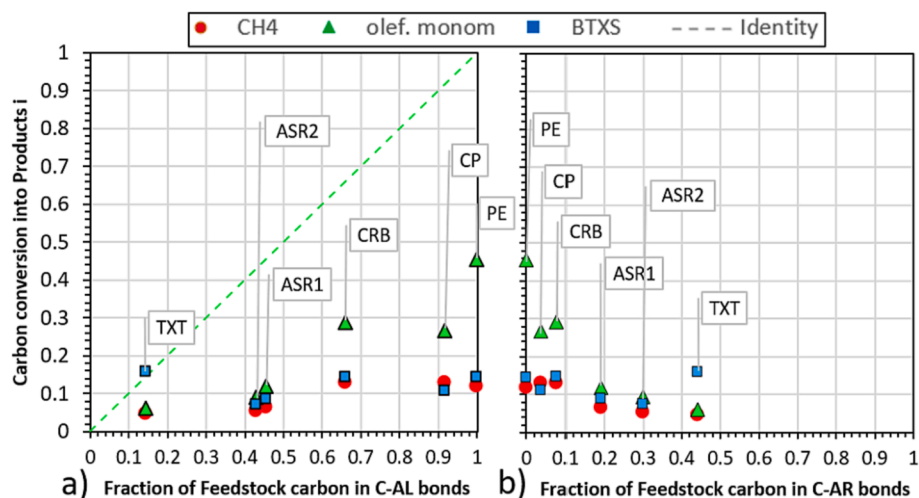


Fig. 11. Carbon conversion into product compound *i* (kgC of species *i* in product per kgC in feedstock) as a function of the fraction of the carbon bond group *j* in the feedstock (kgC in bond type *j* per kgC in feedstock). Carbon Bond group *j* = C-AL, C-AR; product compound *i* = CH₄, olefin monomers, BTXS.

of olefin monomers (green markers) versus C-AL and C-AR. A positive correlation is observed with the aliphatic carbon bonds (C-AL) defined for the material (plot b), indicating the tendency of aliphatics to remain as aliphatics despite the randomness of the free radical-based breakage that they undergo. A negative, and apparently nonlinear, correlation is observed for the aromatic carbons (C-AR), indicating once again the lack of contribution of carbons in rings to the olefin monomer yield. On the other hand, BTXS (blue markers) does not follow clear trends for any of the three groups (plots a, b and c), and it remains almost stable at 0.15. Methane (red markers) is slightly positive correlated with C-AL and the opposite is true for C-AR.

It is noteworthy that in Fig. 10c there is a positive correlation of the aromatics with C-AR, whereas in Fig. 11b there is no obvious correlation for BTXS. This lack of correlation for one-ring aromatics (observed also for C-AL in Fig. 11a) is an indication that more than one route operates to produce these aromatics, with no clearly predominant contributor. In fact, as discussed previously, for some materials the cyclization route prevails, as for instance in the high-polyolefinic materials, while for others the yield arises from direct detachment of the aromatics rings already present in the structure (as is the case for TXT). In relation to the recovery of olefin monomers, a less-steep correlation is observed in Fig. 11a than for the total aliphatics in Fig. 10b (which has a slope closer to the identity line). This is due to C-AL being used to produce other aliphatic components (e.g., CH₄ and others). Nonetheless, it should be noted that the olefin monomer correlation is still close to the aliphatics in Fig. 11b, which may be linked to a higher affinity for C-AL to produce the valuable C₂ and C₃ monomers under the evaluated process conditions.

In general, the framework provided by the carbon bond classification method is not intended to cover the details of the reactions implied, but is instead presented as a way to generalize the complexity of a polymeric blend in a manner such that the influences of certain incoming chemical structures on the outcoming carbon distribution can be investigated easily. Certain potential issues can be improved, for instance the rules established for the carbon bond classification, such that the apparent non-linear behavior observed for TXT could be better resolved. Although further studies with additional materials and conditions are required, these correlations between the defined carbon groups before and after thermal-cracking conversion can open the door for the further development of predictive models that correlate directly with the polymer composition and the process conditions, so as to provide estimations of the potential monomer recovery for a particular material.

6. Conclusions

In this work, four different carbon-based materials, derived from post-consumer rejected waste, were subjected to high-temperature thermo-cracking conditions in an industrial-scale DFB, to determine the potential for the recycling of these materials into molecules with value for the chemical industry and to identify possible correlations between the cracking products and the polymeric composition of the feedstock.

As a preliminary step to the correlation analysis, the shares of different polymers in the complex rejected waste fractions had to be estimated. This estimation was based on an equation system that was formulated and constrained with mass and energy balances. A grid-searching approach was applied to tune the hyper-parameter set of the numerical method. The convex solvers applied, SCS and OSQP, gave similar results, although SCS was found to be more robust for the different polymer compositions tested. The estimations achieved a good degree of numerical approximation using the fractional error function, with errors of <2 % for the elemental balance.

The correlations between the polymer constituents in the feedstock and the cracking products obtained were addressed using a special carbon bond-based classification, accounting for the share of carbons in the feedstock that are bonded to heteroatoms (C-X; X = O, N, S, Cl), in aliphatic bonds (C-AL), and in aromatics (C-AR). The following correlations are identified in this work:

- The olefin monomeric yield presents a positive correlation with the share of feedstock carbon in aliphatic bonds (C-AL), while it shows a negative correlation with the shares of feedstock carbon in C—O and C-AR bonds. This indicates the tendency of aliphatics to persist as aliphatic structures after cracking, as well as the low chance of an aromatic to decompose to yield aliphatics.
- A positive and apparently linear correlation is found between the share of feedstock carbons bonded to oxygen (C—O) and the product yield of CO_x species, while a negative correlation is observed in relation to C-AL in the feedstock.
- A slightly positive correlation is seen for the aromatics produced in relation to C-AR and C—O in the feedstock, although the correlation is negative in relation to C-AL. No clear trend was perceived for BTXS in relation to the defined carbon-bond groups.

The bond-based classification of the carbon atoms in the feedstock allows one to generalize the complexity of the polymeric blend in a common framework that facilitates the identification of certain trends

between the inputs and outputs of the conversion process. Although certain improvements in terms of the carbon classification rules for the feedstock materials can be made, the observed correlations open the way for further explorations of the connections between the characteristics of the carbon bonds in the original material compositions and the final cracking products. Such connections can be exploited in predictive models that provide estimations of monomeric yields from a material based on its polymeric composition and process conditions.

Declaration of Competing Interest

The authors declare that they have no known competing financial interests or personal relationships that could have appeared to influence the work reported in this paper.

Data availability

Data will be made available on request.

Acknowledgments

This work was financially supported by the Stiftelsen Svensk Textiltforskning (Project: Återvinning av textila/polymera material), the project framework Climate-leading Process Industry (Vinnova) (Project: 2018-03012, Återvinning av rejektströmmar från textilsortering och kartongåtervinning), and Borealis AB, Sweden (Project number: 49514-1). The authors thank Jessica Bohwalli, Johannes Öhlin and Rustan Hvitt for technical support during the experiments.

References

- [1] Somoza-Tornos A, Gonzalez-Garay A, Pozo C, Graells M, Espuña A, Guillén-Gosálbez G. Realizing the Potential High Benefits of Circular Economy in the Chemical Industry: Ethylene Monomer Recovery via Polyethylene Pyrolysis. *ACS Sustain Chem Eng* 2020;8:3561–72. <https://doi.org/10.1021/acssuschemeng.9b04835>.
- [2] Datta J, Kopczyńska P. From polymer waste to potential main industrial products: Actual state of recycling and recovering. *Crit Rev Environ Sci Technol* 2016;46: 905–46. <https://doi.org/10.1080/10643389.2016.1180227>.
- [3] Vollmer I, Jenks MJF, Roelands MCP, White RJ, Harmelen T, Wild P, et al. Beyond Mechanical Recycling: Giving New Life to Plastic Waste. *Angew Chem Int Ed* 2020; 59:15402–23. <https://doi.org/10.1002/anie.201915651>.
- [4] Ellen MacArthur Foundation, COMPLETING THE PICTURE: HOW THE CIRCULAR ECONOMY TACKLES CLIMATE CHANGE., www.ellenmacarthurfoundation.org/Publications. (2019).
- [5] IEA. The future of petrochemicals. OECD 2018. <https://doi.org/10.1787/9789264307414-en>.
- [6] Kaminsky W, Predel M, Sadiki A. Feedstock recycling of polymers by pyrolysis in a fluidized bed. *Polym Degrad Stab* 2004;85:1045–50. <https://doi.org/10.1016/J.POLYMEDEGRADSTAB.2003.05.002>.
- [7] OECD, Improving Markets for Recycled Plastics, OECD, 2018. <https://doi.org/10.1787/9789264307414-en>.
- [8] Hahladakis JN, Iacovidou E. Closing the loop on plastic packaging materials: What is quality and how does it affect their circularity? *Sci Total Environ* 2018;630: 1394–400. <https://doi.org/10.1016/J.SCITOTENV.2018.02.330>.
- [9] Thunman H, Berdugo Vilches T, Seemann M, Maric J, Vela IC, Pissot S, et al. Circular use of plastics-transformation of existing petrochemical clusters into thermochemical recycling plants with 100% plastics recovery, Sustainable. *Mater Technol* 2019;22:e00124.
- [10] Neves D, Thunman H, Matos A, Tarelho L, Gómez-Barea A. Characterization and prediction of biomass pyrolysis products. *Prog Energy Combust Sci* 2011;37: 611–30. <https://doi.org/10.1016/j.pecs.2011.01.001>.
- [11] O. Dogu, M. Pelucchi, R. van de Vijver, P.H.M. van Steenberghe, D.R. D'hooge, A. Cuoci, M. Mehl, A. Frassoldati, T. Faravelli, K.M. van Geem, The chemistry of chemical recycling of solid plastic waste via pyrolysis and gasification: State-of-the-art, challenges, and future directions, *Prog Energy Combust Sci*. 84 (2021) 100901. <https://doi.org/10.1016/j.pecs.2020.100901>.
- [12] C. Mandviwala, T. Berdugo Vilches, M. Seemann, R. Faust, H. Thunman, Thermochemical conversion of polyethylene in a fluidized bed: Impact of transition metal-induced oxygen transport on product distribution, *J Anal Appl Pyrolysis*. 163 (2022). <https://doi.org/10.1016/j.jaap.2022.105476>.
- [13] Jung SH, Cho MH, Kang BS, Kim JS. Pyrolysis of a fraction of waste polypropylene and polyethylene for the recovery of BTX aromatics using a fluidized bed reactor. *Fuel Process Technol* 2010;91:277–84. <https://doi.org/10.1016/J.FUPROC.2009.10.009>.
- [14] Kaminsky W, Kim JS. Pyrolysis of mixed plastics into aromatics. *J Anal Appl Pyrolysis* 1999;51:127–34. [https://doi.org/10.1016/S0165-2370\(99\)00012-1](https://doi.org/10.1016/S0165-2370(99)00012-1).
- [15] Zhou H, Wu C, Onwudili JA, Meng A, Zhang Y, Williams PT. Influence of process conditions on the formation of 2–4 ring polycyclic aromatic hydrocarbons from the pyrolysis of polyvinyl chloride. *Fuel Process Technol* 2016;144:299–304. <https://doi.org/10.1016/J.FUPROC.2016.01.013>.
- [16] Pfeifer C, Koppatz S, Hofbauer H. Steam gasification of various feedstocks at a dual fluidized bed gasifier: Impacts of operation conditions and bed materials. *Biomass Convers Biorefin* 2011;1:39–53. <https://doi.org/10.1007/s13399-011-0007-1>.
- [17] Thunman H, Seemann M, Berdugo Vilches T, Maric J, Pallares D, Ström H, et al. Advanced biofuel production via gasification - lessons learned from 200 man-years of research activity with Chalmers' research gasifier and the GoBiGas demonstration plant. *Energy Sci Eng* 2018;6:6–34. <https://doi.org/10.1002/ese3.188>.
- [18] Wilk V, Hofbauer H. Conversion of mixed plastic wastes in a dual fluidized bed steam gasifier. *Fuel* 2013;107:787–99. <https://doi.org/10.1016/J.FUEL.2013.01.068>.
- [19] Sadeghbeigi R, Chapter., 1 - Process Description. *Fluid Catalytic Cracking Handbook* 2000:1–39. <https://doi.org/10.1016/B978-088415289-7/50002-0>.
- [20] Karl J. Biomass heat pipe reformer—design and performance of an indirectly heated steam gasifier. *Biomass Convers Biorefin* 2014;4:1–14. <https://doi.org/10.1007/s13399-013-0102-6>.
- [21] Cañete Vela I, Berdugo Vilches T, Berndes G, Johnsson F, Thunman H. Co-recycling of natural and synthetic carbon materials for a sustainable circular economy. *J Clean Prod* 2022;365:132674. <https://doi.org/10.1016/J.JCLEPRO.2022.132674>.
- [22] Wu C, Williams PT. Pyrolysis–gasification of plastics, mixed plastics and real-world plastic waste with and without Ni–Mg–Al catalyst. *Fuel* 2010;89:3022–32. <https://doi.org/10.1016/J.FUEL.2010.05.032>.
- [23] Kaminsky W, Schlesselmann B, Simon C. Olefins from polyolefins and mixed plastics by pyrolysis. *J Anal Appl Pyrolysis* 1995;32:19–27. [https://doi.org/10.1016/0165-2370\(94\)00830-T](https://doi.org/10.1016/0165-2370(94)00830-T).
- [24] Wu X, Li J, Yao L, Xu Z. Auto-sorting commonly recovered plastics from waste household appliances and electronics using near-infrared spectroscopy. *J Clean Prod* 2020;246:118732. <https://doi.org/10.1016/j.jclepro.2019.118732>.
- [25] Zada L, Leslie HA, Vethaak AD, Tinnevelt GH, Jansen JJ, de Boer JF, et al. Fast microplastics identification with stimulated Raman scattering microscopy. *J Raman Spectrosc* 2018;49:1136–44. <https://doi.org/10.1002/jrs.5367>.
- [26] Adarsh UK, Bhoje Gowd E, Bankapur A, Kartha VB, Chidangil S, Unnikrishnan VK. Development of an inter-confirmatory plastic characterization system using spectroscopic techniques for waste management. *Waste Manag* 2022;150:339–51. <https://doi.org/10.1016/j.wasman.2022.07.025>.
- [27] Netzer C, Li T, Lovås T. Surrogate Reaction Mechanism for Waste Incineration and Pollutant Formation. *Energy Fuel* 2021;35:7030–49. <https://doi.org/10.1021/acs.energyfuels.0c03485>.
- [28] W. Kaminsky, The Hamburg Fluidized-bed Pyrolysis Process to Recycle Polymer Wastes and Tires, in: *Feedstock Recycling and Pyrolysis of Waste Plastics*, John Wiley & Sons, Ltd, 2006: pp. 475–491. <https://doi.org/10.1002/0470021543.ch17>.
- [29] E. Akca, A. Gursel, N. Sen, A review on devulcanization of waste tire rubber, *Periodicals of Engineering and Natural Sciences (PEN)*. 6 (2018) 154. <https://doi.org/10.21533/pen.v6i1.167>.
- [30] Landi D, Vitali S, Germani M. Environmental Analysis of Different End of Life Scenarios of Tires Textile Fibers. *Procedia CIRP* 2016;48:508–13. <https://doi.org/10.1016/J.PROCIRP.2016.03.141>.
- [31] Formela K, Hejna A, Zedler L, Colom X, Canavate J. Microwave treatment in waste rubber recycling – recent advances and limitations. *Express Polym Lett* 2019;13: 565–88. <https://doi.org/10.3144/expresspolymlett.2019.48>.
- [32] Zhou H, Meng A, Long Y, Li Q, Zhang Y. Classification and comparison of municipal solid waste based on thermochemical characteristics. *J Air Waste Manage Assoc* 2014;64:597–616. <https://doi.org/10.1080/10962247.2013.873094>.
- [33] Abbas-Abadi MS. The effect of process and structural parameters on the stability, thermo-mechanical and thermal degradation of polymers with hydrocarbon skeleton containing PE, PP, PS, PVC, NR, PBR and SBR. *J Therm Anal Calorim* 2021;143:2867–82. <https://doi.org/10.1007/s10973-020-09344-0>.
- [34] Scheirs J, Kaminsky W, editors. *Feedstock Recycling and Pyrolysis of Waste Plastics: Converting Waste Plastics into Diesel and Other Fuels*. Wiley; 2006. <https://doi.org/10.1002/0470021543>.
- [35] Miskolczi N, Bartha L, Angyal A. Pyrolysis of Polyvinyl Chloride (PVC)-Containing Mixed Plastic Wastes for Recovery of Hydrocarbons. *Energy Fuel* 2009;23:2743–9. <https://doi.org/10.1021/ef8011245>.
- [36] Gebre SH, Sendeku MG, Bahri M. Recent Trends in the Pyrolysis of Non-Degradable Waste Plastics. *ChemistryOpen* 2021;10:1202–26. <https://doi.org/10.1002/open.202100184>.
- [37] Martín-Gullón I, Esperanza M, Font R. Kinetic model for the pyrolysis and combustion of poly-(ethylene terephthalate) (PET). *J Anal Appl Pyrolysis* 2001; 58–59:635–50. [https://doi.org/10.1016/S0165-2370\(00\)00141-8](https://doi.org/10.1016/S0165-2370(00)00141-8).
- [38] Das P, Tiwari P. Thermal degradation study of waste polyethylene terephthalate (PET) under inert and oxidative environments. *Thermochim Acta* 2019;679: 178340. <https://doi.org/10.1016/J.TCA.2019.178340>.
- [39] Maric J, Berdugo Vilches T, Pissot S, Cañete Vela I, Gyllenhammar M, Seemann M. Emissions of dioxins and furans during steam gasification of Automotive Shredder residue; experiences from the Chalmers 2–4-MW indirect gasifier. *Waste Manag* 2020;102:114–21. <https://doi.org/10.1016/j.wasman.2019.10.037>.
- [40] Herrera M, Matuschek G, Ketrup A. Main products and kinetics of the thermal degradation of polyamides. *Chemosphere* 2001;42:601–7. [https://doi.org/10.1016/S0045-6535\(00\)00233-2](https://doi.org/10.1016/S0045-6535(00)00233-2).

- [41] Nielsen M, Jurasek P, Hayashi J, Furimsky E. Formation of toxic gases during pyrolysis of polyacrylonitrile and nylons. *J Anal Appl Pyrolysis* 1995;35:43–51. [https://doi.org/10.1016/0165-2370\(95\)00898-0](https://doi.org/10.1016/0165-2370(95)00898-0).
- [42] Shen DK, Gu S. The mechanism for thermal decomposition of cellulose and its main products. *Bioresour Technol* 2009;100:6496–504. <https://doi.org/10.1016/J.BIORTECH.2009.06.095>.
- [43] Williams PT, Williams EA. Interaction of Plastics in Mixed-Plastics Pyrolysis. *Energy Fuel* 1999;13:188–96. <https://doi.org/10.1021/ef980163x>.
- [44] Stanmore BR. The formation of dioxins in combustion systems. *Combust Flame* 2004;136:398–427. <https://doi.org/10.1016/J.COMBUSTFLAME.2003.11.004>.
- [45] Masoumeh Safavi S, Richter C, Unnthorsson R. Gasification [Working Title]. *IntechOpen*; 2021.
- [46] Safavi A, Richter C, Unnthorsson R. Dioxin Formation in Biomass Gasification: A Review. *Energies (Basel)* 2022;15:700. <https://doi.org/10.3390/en15030700>.
- [47] S. Boyd, L. Vandenberghe, *Convex Optimization*, (2009). <http://www.cambridge.org> (accessed October 12, 2022).
- [48] Beck A. *First-Order Methods in Optimization*. Philadelphia, PA, USA: SIAM-Society for Industrial and Applied Mathematics; 2017.
- [49] Dvurechensky P, Shtern S, Staudigl M. First-Order Methods for Convex Optimization. *EURO Journal on Computational Optimization* 2021;9:100015. <https://doi.org/10.1016/J.EJCO.2021.100015>.
- [50] B. O'Donoghue, Operator splitting for a homogeneous embedding of the linear complementarity problem, (2020). <https://doi.org/10.48550/arxiv.2004.02177>.
- [51] SCS — SCS 3.2.1 documentation, (n.d.). <https://www.cvxgrp.org/scs/> (accessed October 12, 2022).
- [52] Stellato B, Banjac G, Goulart P, Bemporad A, Boyd S. OSQP: an operator splitting solver for quadratic programs. *Math Program Comput* 2020;12:637–72. <https://doi.org/10.1007/s12532-020-00179-2>.
- [53] The solver — OSQP documentation, (n.d.). <https://osqp.org/docs/solver/index.html> (accessed October 12, 2022).
- [54] Diamond S, Boyd S. CVXPY: A Python-Embedded Modeling Language for Convex Optimization. *J Mach Learn Res* 2016;17:2909–13.
- [55] Agrawal A, Verschueren R, Diamond S, Boyd S. A rewriting system for convex optimization problems. *Journal of Control and Decision* 2018;5:42–60. <https://doi.org/10.1080/23307706.2017.1397554>.
- [56] Grid Search for model tuning. A model hyperparameter is a... | by Rohan Joseph | Towards Data Science, (n.d.). <https://towardsdatascience.com/grid-search-for-model-tuning-3319b259367e> (accessed October 12, 2022).
- [57] Larsson A, Seemann M, Neves D, Thunman H. Evaluation of Performance of Industrial-Scale Dual Fluidized Bed Gasifiers Using the Chalmers 2–4-MW_{th} Gasifier. *Energy Fuel* 2013;27:6665–80. <https://doi.org/10.1021/ef400981j>.
- [58] Berdugo Vilches T, Thunman H. Experimental Investigation of Volatiles-Bed Contact in a 2–4 MW_{th} Bubbling Bed Reactor of a Dual Fluidized Bed Gasifier. *Energy Fuel* 2015;29:6456–64. <https://doi.org/10.1021/acs.energyfuels.5b01303>.
- [59] Israelsson M, Larsson A, Thunman H. Online Measurement of Elemental Yields, Oxygen Transport, Condensable Compounds, and Heating Values in Gasification Systems. *Energy Fuel* 2014;28:5892–901. <https://doi.org/10.1021/ef501433n>.
- [60] Pissot S, Berdugo Vilches T, Maric J, Cañete Vela I, Thunman H, Seemann M. Thermochemical Recycling of Automotive Shredder Residue by Chemical-Looping Gasification Using the Generated Ash as Oxygen Carrier. *Energy Fuel* 2019;33:11552–66. <https://doi.org/10.1021/acs.energyfuels.9b02607>.